RESEARCH ARTICLE

Journal of Optics and Photonics Research 2025, Vol. 00(00) 1–9

DOI: 10.47852/bonviewJOPR52024917



Deep Learning and LPF-Based Decision Technique in Free-Space Optical Communication Links

Yan Gao¹, Yan-Qing Hong^{1,*}, Chao-Yue Zhai¹ and Xiao-Xue Ren¹

¹School of Information Science and Engineering, Shenyang University of Technology, China

Abstract: This study proposes a threshold decision technology to compensate for the turbulence effect in free-space optical (FSO) communication links, which integrates deep learning (DL) with a low-pass filter (LPF) to enhance system performance. Firstly, we introduce DL model of fully connected neural network (FCNN) for the sake of adaptive threshold decision (ATD) capability improvement. Then, in the cascaded LPF and FCNN approach, in order to improve the accuracy of channel state information (CSI) signal acquired from LPF, FCNN model is deployed behind LPF with a fixed cut-off frequency set for different turbulence channel degrees and data rates. For the adaptive cut-off frequency scheme of FCNN-based LPF technology, we utilize the FCNN model to determine the cut-off frequency value of LPF according to the estimated turbulence channel characteristics, enabling flexible variation of cut-off frequency values across diverse turbulence channel degrees and data rates. Finally, we conducted simulations to evaluate this technology. Simulation results demonstrate that FCNN-based adaptive cut-off frequency LPF technology outperforms LPF-based ATD with a fixed cut-off frequency, the FCNN-based ATD, and our proposed cascaded LPF and FCNN approach. Furthermore, its performance is approximate to theoretical ATD with comprehensive CSI knowledge. Therefore, the proposed method is a promising solution to compensate turbulence effect in FSO links.

Keywords: deep learning, threshold decision, turbulence channel, free-space optical communication link

1. Introduction

The free-space optical (FSO) communication system has emerged as a highly attractive alternative to address the limitations imposed by radio frequency (RF) bandwidth saturation [1]. With unique attributes such as exemption from licensing, straightforward deployment, and a heightened security profile due to reduced detectability, FSO has become a notable contender for applications ranging from initial network access to emergency communication recovery [2]. However, as a result of the heterogeneous distributional attributes of the atmospheric refractive index, the optical signal in transit encounters significant intensity variations upon reaching the receiver, a phenomenon commonly referred to as the scintillation effect [3]. This turbulence-generated effect significantly degrades the capacity of optical communication link and limits the development of FSO communication technology.

To address the issue of scintillation effect, researchers have developed various technologies, including adaptive optics, saturated optical amplifiers, polarization modulation, diversity techniques, and adaptive threshold decision (ATD), among others [4–6]. Among them, the ATD method has garnered significant attention due to its simplicity. Researchers have explored the application of ATD in mitigating scintillation effect on the basis of estimating thresholds symbol-by-symbol [7]. However, in order to make optimal

decisions, the high precision degree of channel state information (CSI) is required, i.e., the knowledge of time-varying signal intensity variation [8]. Given the low-frequency spectrum features of turbulent channels, researchers have used well-configured low-pass filters (LPF) to fetch the CSI signal from the received signal [9, 10]. However, it should be noted that in the case of low-speed signal transmission, the performance of this method can be severely impacted due to a significant reduction in CSI signal accuracy. To this end, researchers have studied a block-based multi-symbol threshold decision method that optimizes periodic decision threshold for a block-wise received signal utilizing incomplete CSI knowledge [11]. Yet, determining the specific scope of this incompleteness remains a challenge.

In the face of the challenges posed by conventional signal processing methods, efforts are currently being conducted to introduce deep learning (DL) technologies into FSO links [12–14]. A universal artificial neural network (ANN) has been proposed to classify analog and digital modulation formats using the nine key features [15]. Nonetheless, the applicability of the neural network model hinges on the process of the training data, which may influence it to fall into local optimums. Additionally, a deep neural network (DNN) model was adopted to demodulate received signals under conditions of incomplete CSI [16]. It is worth noting that different turbulent channels require different weight configurations. The receiver structure in line with fully connected deep neural network (FC-DNN) model has been studied for achieving synchronization and recovery of received signals in underwater optical wireless communication [17].

^{*}Corresponding author: Yan-Qing Hong, School of Information Science and Engineering, Shenyang University of Technology, China. Email: hongy7@sut.edu.cn

[©] The Author(s) 2025. Published by BON VIEW PUBLISHING PTE. LTD. This is an open access article under the CC BY License (https://creativecommons.org/licenses/by/4.0/).

Furthermore, a convolutional neural network (CNN) model has been introduced to identify the degree of turbulence and mode of orbital angular momentum [18–20]. However, this method increases the complexity of transmitters and receivers. With an understanding of fully connected neural networks (FCNN), the use of channel parameters has been explored to differentiate received on-off keying (OOK) signals [21]. Yet, due to the imbalance features of class in the dataset, the accuracy of predictions may decrease. Therefore, it is particularly important to explore the application of DL technologies to develop an efficient ATD method.

In this work, DL and LPF-based decision method is proposed in FSO links. Since the scintillation effect is mainly composed of low-frequency spectral components, the CSI signal can be filtered out from the receiving signal using a LPF. Manchester on-off keying (M-OOK) is adopted as to enhance the CSI signal accuracy extracted by the LPF. The receiving M-OOK signal is split into two parts: one for extracting CSI signal and the other for demodulation. To increase the accuracy degree of CSI extracted by the LPF across different turbulent channels and data rates, a FCNN model is employed. Two DL-assisted approaches are proposed. The first is the cascaded LPF and FCNN method, which deploys the FCNN model following LPF configuring the fixed cut-off frequency as to enhance the accuracy of CSI knowledge extracted by the LPF. The second is the adaptive cut-off frequency based on FCNN for LPF technology, which uses FCNN model to determine the cut-off frequency value of LPF based on the estimated characteristics of the turbulent channel. This technique is compared with LPF-based ATD with a fixed LPF cut-off frequency, FCNN-based ATD, and theoretical ATD with perfect CSI knowledge. Simulation results show that the proposed FCNN-based adaptive cut-off frequency LPF technology outperforms LPF-based ATD with a fixed LPF cut-off frequency, FCNN-based ATD, and the proposed cascaded LPF and FCNN method. Furthermore, its performance is approximate to theoretical ATD under ideal CSI knowledge.

2. Principle of Operation

Figure 1 shows the block diagram of the proposed technique. In this technique, direct modulation and 1550 nanometers laser diode (LD) are adopted. Compared to OOK, the application of M-OOK signals can reduce signal distortion in the low-pass filter (LPF) caused by missing low-frequency features. The transmitted M-OOK signal s(t) is represented by [22]

$$s(t) = \sum_{k=-\infty}^{\infty} d[k]g(t - kT) \tag{1}$$

where T, d[k], and g(t) are symbol period, data sequence, and square-wave shaping pulse respectively. When the optical signal traverses an atmospheric turbulence channel, due to the random fluctuation characteristics of temperature and pressure, the optical signal undergoes significant distortion severely impacted by turbulence effects [4]. Among these turbulence effects, the scintillation induced by turbulence leads to intense optical irradiation variation. It is the major issue in FSO system and usually evaluated using the scintillation index σ_1^2 . Besides, high value of σ_1^2 indicates a serious signal intensity fluctuation phenomenon. σ_1^2 is given by

$$\sigma_I^2 = \frac{\langle I^2 \rangle}{\langle I \rangle^2} - 1 \tag{2}$$

where I and $\langle . \rangle$ are the intensity of receiving signal and symbol of ensemble average respectively [23]. The receiving optical signal is transformed into electrical signal using photodiode (PD) alongside the noise generation during the detection process. Then, analog r(t) to digital r[k] conversion process is accomplished, and it is given by [24]

$$r[k] = I[k]s[k] + N[k]$$
(3)

where N[k] is additive white Gaussian noise (AWGN). In order to handle scintillation effect, we propose DL-assisted LPF-based ATD approaches, i.e., the cascaded LPF and FCNN, and adaptive LPF cut-off frequency based on FCNN.

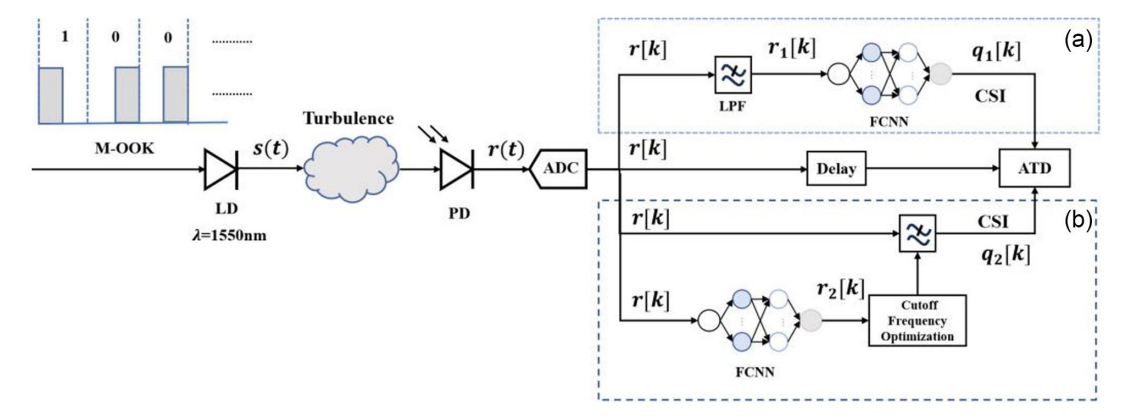
2.1. Cascaded LPF and FCNN

Figure 1(a) shows the proposed Cascaded LPF and FCNN method. In this method, receiving signal is split into two parts. One part utilizes the LPF and FCNN model to acquire CSI knowledge of the turbulent channel. For the other branch, which is the lower one, time delay is carried out to ensure synchronization between two paths. The output signal of LPF $r_1[k]$ is expressed as

$$r_1[k] = r[k]h[k] \tag{4}$$

where h[k] is LPF impulse response. Frequency domain of h[k] is shown as

Figure 1
Block diagram of (a) LPF and FCNN cascading and (b) adaptive LPF cut-off frequency based on FCNN



$$H(\omega) = \sum h[k] \cdot e^{(-j\omega k)} \tag{5}$$

where ω depicts angular frequency. Cut-off frequency ω_c of LPF is given by [25]

$$\omega_c = 1/\left(\tau\sqrt{\left(2^{(1/O)} - 1\right)}\right) \tag{6}$$

where τ and O are the nominal bandwidth and order of the LPF respectively. $H(\omega_c)$ is calculated by [25]

$$H(\omega_c) = 1/(1 + (\omega_n/\omega_c)^{(2*O)})$$
 (7)

where ω_n represents normalized frequency. As to LPF, the cut-off frequency is dynamically adjusted in order to obtain CSI signal with high accuracy under various turbulence degrees and data rates [10]. Thus, FCNN model is adopted associated with LPF to realize an effective CSI estimation under LPF with a fixed cut-off frequency. The basic FCNN model is deployed in this work, since it is sufficient to process the features of received signal. FCNN model is composed of one input, two hidden, and one output layers as shown in Figure 2. The input signal $\mathbf{r}_1[\mathbf{k}]$ transparently passes through modified input layer into hidden layer. The rectified linear unit (ReLU) plays the role of activation function to achieve nonlinear transformation in hidden layer, which transforms by learning the nonlinear feature representation of $\mathbf{r}_1[\mathbf{k}]$. Subsequently, the spectrum of the output signal is reconstructed by these learned feature representations in the output layer. The processes of input, hidden, and output layers are represented by [26]

$$L_1[k] = R(w_1 r_1[k] + b_1),$$

$$L_2[k] = R(w_2 L_1[k] + b_2),$$

$$q_1[k] = R(w_3 L_2[k] + b_3)$$
(8)

where w_i is the weight matrix of the layer i, b_i is the bias term of the layer i, L_1 is the input layer, L_2 represents a neural network structure composed by two hidden layers, R denotes ReLU-based activation function, and q_1 is the output layer. $q_1[k]$ is obtained through a prediction process of the CSI signal and is utilized as the decision threshold for implementing the ATD scheme. Mean squared error (MSE) is applied as loss function to measure the accuracy, and it is calculated by [27]

$$MSE = \sum ((r_2 - r_P)^2)/k$$
 (9)

Input Hidden Hidden Output Layer ϵR^1 Layer ϵR^3 Layer ϵR^3 Layer ϵR^1

Figure 2

where k is the index of the sample. The error probability P_e is analyzed to evaluate the capability of decision method, and P_e is given by

$$P_{e} = P(0) \cdot P(1|0) + P(1) \cdot P(0|1) \tag{10}$$

where the conditional error probabilities are represented by P(1|0) and P(0|1) respectively. P(0) and P(1) are supposed to 0.5, and BER₁ is calculated by [23]

$$BER_{1} = \frac{1}{4} erfc \left(\frac{r - \langle U_{0} \rangle}{\sqrt{2\sigma_{0}^{2}}} \right) + \frac{1}{4} erfc \left(\frac{\langle U_{1} \rangle - r}{\sqrt{2\sigma_{1}^{2}}} \right), \tag{11}$$

where $erfc(\cdot)$ shows the complementary error function. $\langle U_1 \rangle$ and σ_1^2 are mean and variance values, respectively.

2.2. FCNN-based adaptive cut-off frequency of LPF

Figure 1(b) shows the proposed FCNN-based adaptive cut-off frequency of LPF method. In this proposed mechanism, the received signal is split into three branches, with an added delay in the upper branch to ensure synchronization with signals from other paths. The middle branch utilizes an LPF with the capability of dynamically adjusting its cut-off frequency to extract CSI signals from the receiving signal. As to LPF, the cut-off frequency is adaptively selected by the lower branch using FCNN model by learning the frequency characteristics of the received signal as to increase the accuracy of extracted CSI. The input signal r[k] is delivered into the hidden layers through modified input layer. The frequency domain features of r[k] learned by ReLU by the process of nonlinear transformations. The frequency spectrum of $r_2[k]$ is rebuilt in output layer by learning the frequency domain features. In Figure 3, the maximum spectral component ω_{c_0} is selected in the process of cut-off frequency optimization process, and ω_{c_0} is set as the optimal LPF cut-off frequency. It is calculated by

$$\omega_{c_{\alpha}} = \max(|C(e^{j\omega})|) \tag{12}$$

where $C(e^{j\omega})$ shows frequency spectrum of $r_2[k]$.

The CSI signal $q_2(\omega)$ is acquired via LPF with the selected cutoff frequency. This acquisition process is shown by

Figure 3
Optimized cut-off frequency selection

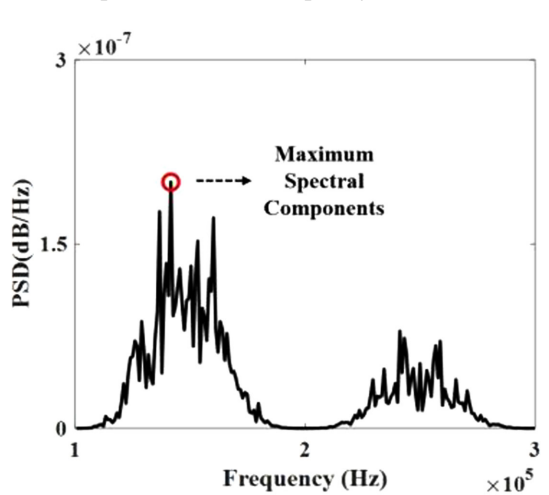
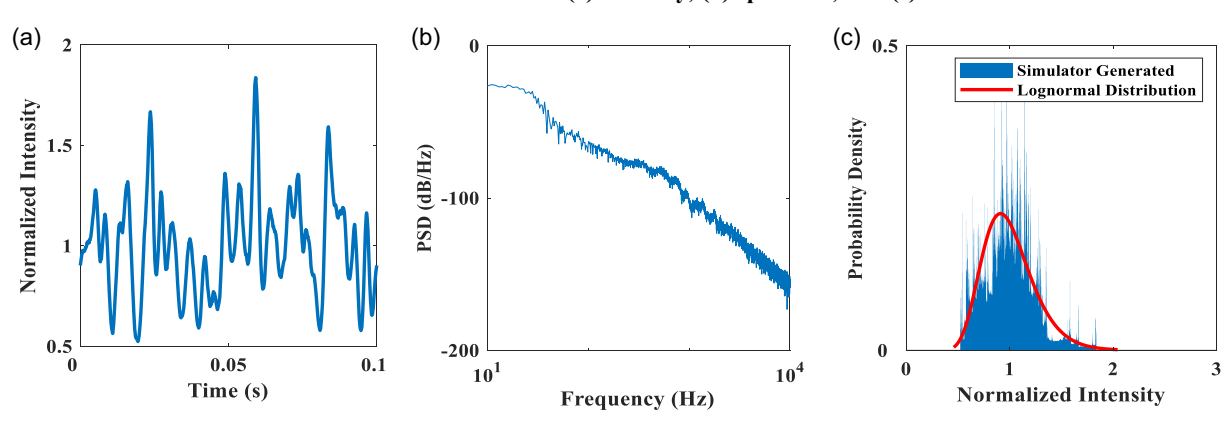


Figure 4
Modeled turbulence channel: (a) intensity, (b) spectrum, and (c) PDF



 $q_2(\omega) = R(\omega)H_o(\omega) \tag{13}$

where frequency domain of r[k] is represented by $R(\omega)$. Finally, ATD is realized using estimated CSI signal $q_2[k]$, which plays the role of the decision thresholds. The degree of accuracy is estimated by MSE in Equation (9) as well. The BER₂ is expressed as

$$BER_{2} = \frac{1}{4} erfc \left(\frac{r - \langle U_{0} \rangle}{\sqrt{2\sigma_{0}^{2}}} \right) + \frac{1}{4} erfc \left(\frac{\langle U_{1} \rangle - r}{\sqrt{2\sigma_{I}^{2}}} \right)$$
(14)

Therefore, the scintillation effect is effectively mitigated through cascading LPF and FCNN, as well as the adaptive cut-off frequency technique based on FCNN-enabled LPF.

3. Channel Modeling

In this work, the log-normal distribution is utilized to accommodate the scintillation effect based on the characteristics of time-varying intensity variations. The log-normal distribution is commonly utilized to express weak turbulence channel on account of its simplicity and widespread application. The probability density function (PDF) of the log-normal distribution is calculated as [24]

$$f(I) = \frac{1}{\sqrt{2\pi\sigma_I^2}} \exp\left[-\frac{(\ln(I) - \mu)^2}{2\sigma_I^2}\right]$$
 (15)

where μ is the mean of $\ln(I)$. The time-varying intensity variations with a log-normal distribution are derived from the time spectrum of log-normal amplitude variations. In the context of weak turbulence channels, it is depicted by [25, 26]

$$W_{D}(f) = 0.528\pi^{2}k^{2} \int_{I} C_{n}^{2}(H) \int_{-\infty}^{\infty} \frac{\nu(H)}{[(\kappa\nu(H))^{2} - (2\pi f)^{2}]^{\frac{1}{2}}} sin^{2} \left(\frac{\kappa\gamma H}{2k}\right) F(\gamma\kappa) d\kappa dH,$$
(16)

where D represents log-amplitude, l is the distance of communication link, H is the transmitter altitude, C_n^2 is the refractive index structure based on the model of Hufnagel-Valley, ν represents wind velocity model, $\kappa=2\pi/\lambda$ is the number of optical wave, k represents spatial wave number, and $F(\cdot)$ is the function of aperture filter. The information of phase is randomly added into $W_D(f)$. Then, it is converted into time domain using Fourier inverse transform. Through the above process, we finally obtain a turbulent channel with scintillation effect. Figure 4 shows the simulated turbulent channel when σ_1^2 is 0.0596. Figure 4(a) shows the

intensity variation features of the modeling channel, and the time-varying signal intensity alteration was observed. Figure 4(b) shows the spectrum of the modeled turbulence channel, and it is obvious that low-frequency components dominate in spectrum. Figure 4(c) presents the distribution feature of the simulated turbulent channel, with its distribution curve matching the log-normal distribution. Therefore, we have effectively established a model of the turbulent channel and used it as the training dataset for this study, and channel attenuation coefficient and background noises were ignored.

4. Simulations and Results

In simulation, the proposed DL and LPF-based decision method was validated. ATD with accurate CSI, ATD with a single LPF using a fixed LPF cut-off frequency, ATD based on a single FCNN, and the proposed cascaded LPF and FCNN with adaptive cut-off frequency based on FCNN were compared under various data rates and turbulent channels. Besides, the degree of computational complexity and accuracy were also analyzed between different methods. The noise equivalent power was configured into 5×10^{-14} W/Hz for PD. LPF was set according to the specifications illustrated in Table 1 [28]. FCNN model was configured as to parameters depicted in Table 2, and training and testing of dataset were set 80% and 20% respectively. The simulations were carried out on a laptop equipped with an NVIDIA GeForce RTX 3050 GPU.

Table 1 LPF parameters

Туре	Passband attenuation	Stopband attenuation
Butterworth	3 dB	30 dB

Table 2
The tuned hyperparameters

Hyperparameters	Values
Dataset size	10 Mbps = 1×10^7 , 50 Mbps = 5×10^7
Dataset size-training	10 Mbps = 8×10^6 , 50 Mbps = 4×10^7
Dataset size-testing	10 Mbps = 2×10^5 , 50 Mbps = 1×10^6
Function of activation	ReLU
Function of loss	MSE
Epoch	20
Batch-size	500
Learning rate	0.001
Turbulence intensity	$\sigma_I^2 = 0.7248, 0.4286, 0.2080, 0.0596$

Figure 5 displays the BERs of ATD using single LPF at different cut-off frequencies of the LPF, where the CSI signal is obtained through LPF filtering. The data rates for M-OOK modulation were configured into 10 Mbps and 50 Mbps,

respectively. The average signal-to-noise ratio (SNR) was fixed at a high value to reduce the impact of PD noise. The simulations were employed by turbulent channels with scintillation effects at $\sigma_{\rm L}^2$ values of 0.0596 and 0.4286. On account of turbulent channel

Figure 5
BERs of ATD using single LPF with different cut-off frequencies

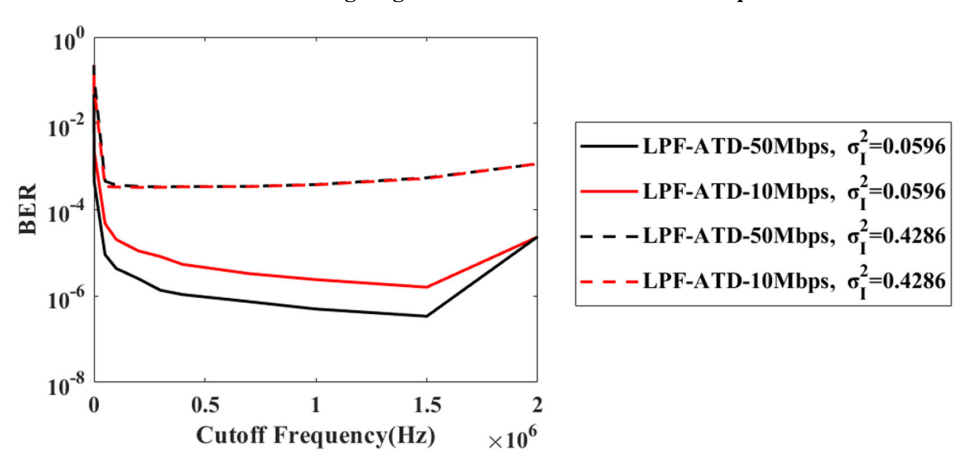
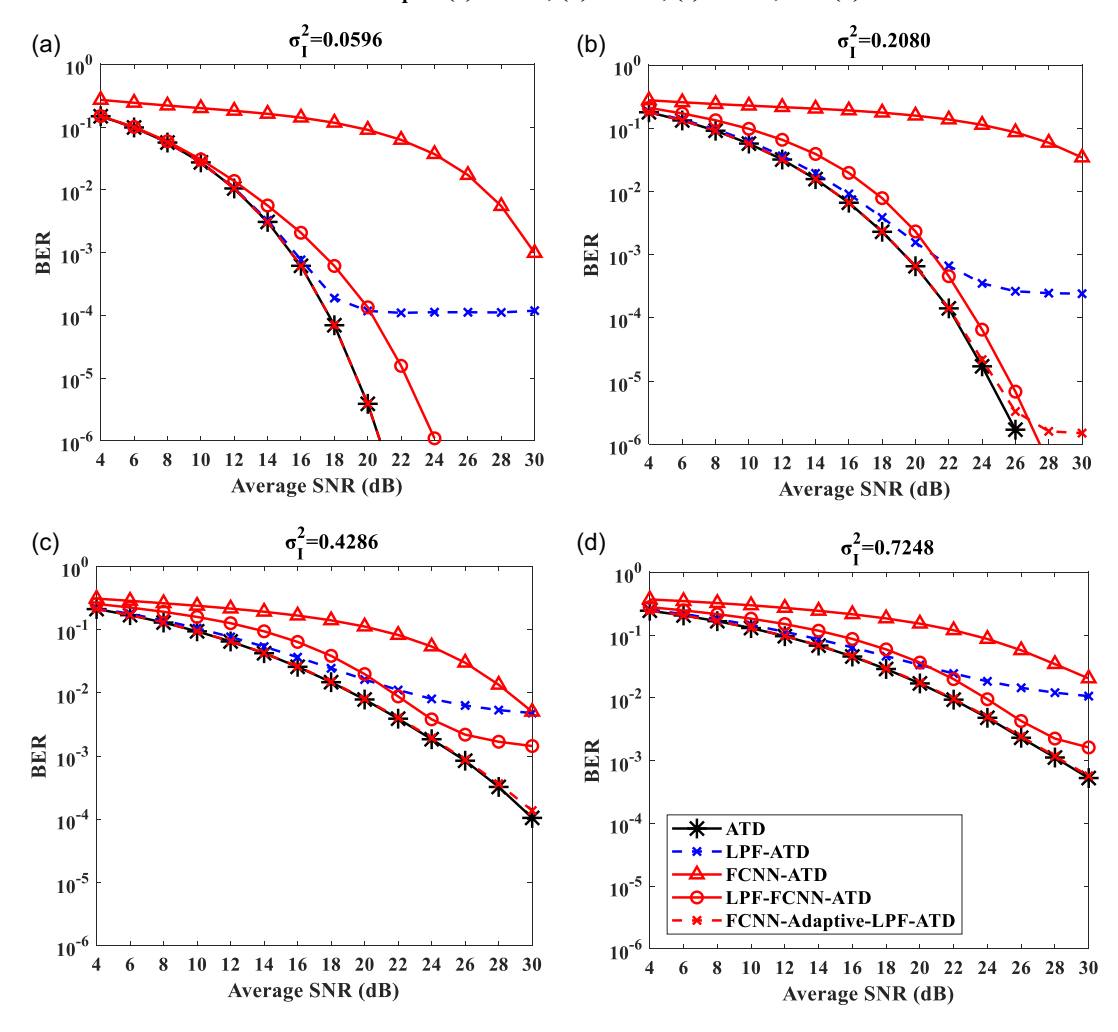
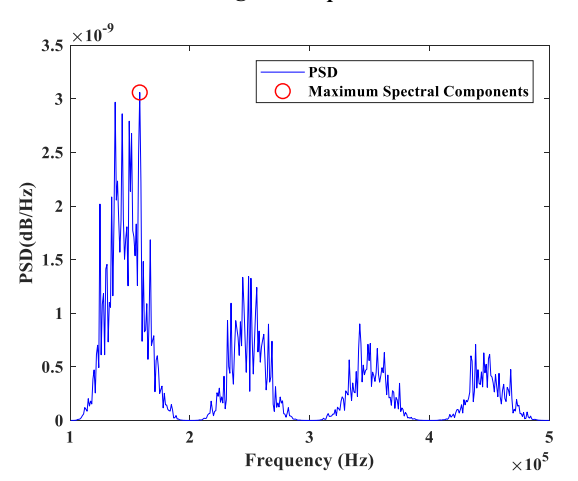


Figure 6 BERs of various threshold decision methods at $\sigma_{\rm I}^2$ of (a) 0.0596, (b) 0.2080, (c) 0.4286, and (d) 0.7248 at the data rate of 10 Mbps.



Note: FCNN-ATD: ATD based on single FCNN; LPF-FCNN-ATD: ATD based on LPF and FCNN cascading; FCNN-Adaptive-LPF-ATD: FCNN-based adaptive LPF cut-off frequency

Figure 7 Optimized cut-off frequency selection in the spectrum of received M-OOK signal at σ_1^2 of 0.0596

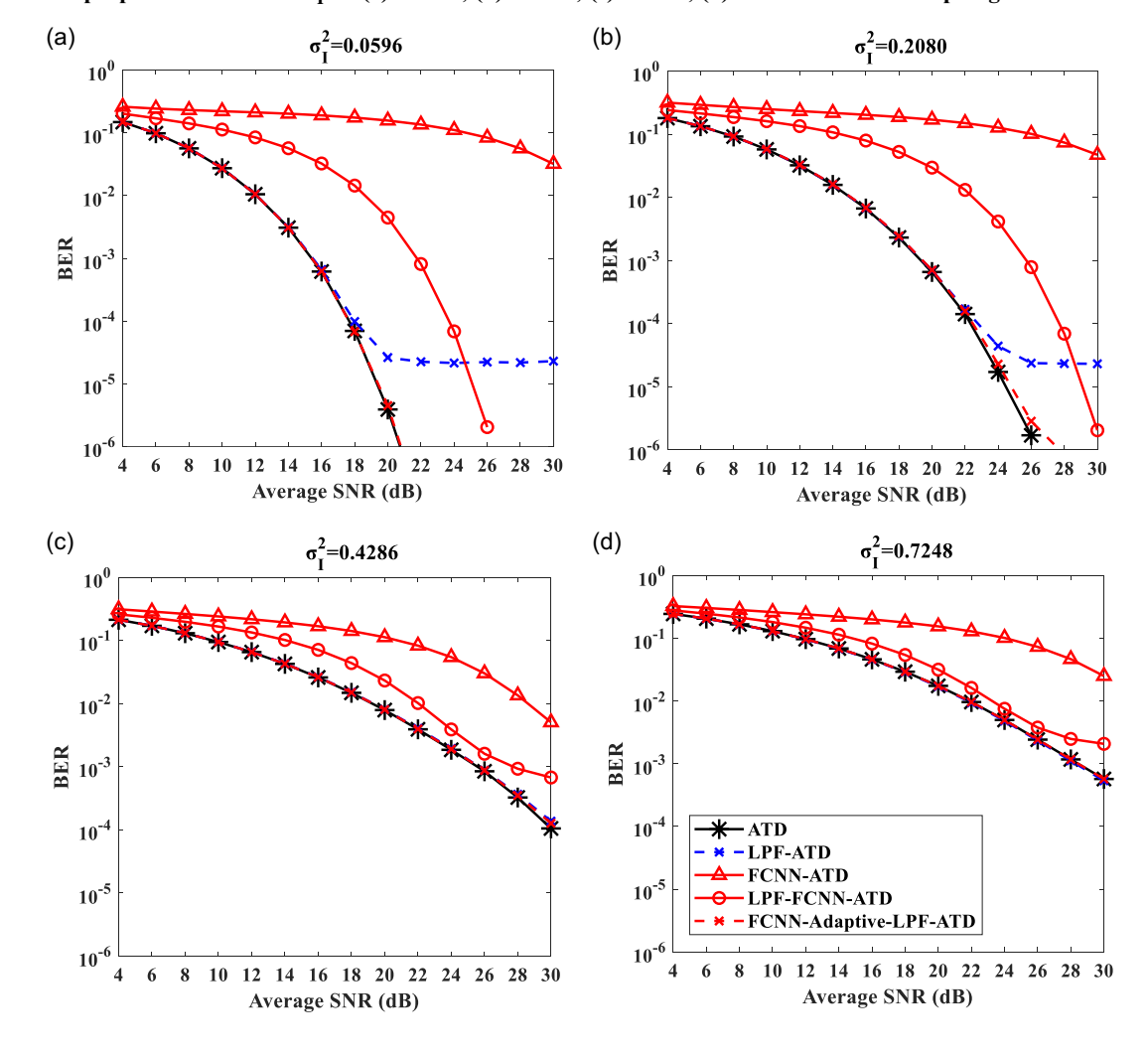


possessed with low-frequency features, the cut-off frequency of LPF was set from 0 Hz to 2×10^6 Hz. For M-OOK signal with 10 Mbps transmission, when cut-off frequency was increased, the accuracy of

the CSI knowledge was increased through the acquisition of a larger number of turbulent channel frequency components. However, the decrease of BER was observed under circumstance of exceeding a critical cut-off frequency point by the reason of larger quantity of M-OOK signal component addition. A similar relationship between BER and cut-off frequency was observed at M-OOK signal transmission with data rate of 50 Mbps. Besides, it has a better BER performance and wider range of permitted cut-off frequencies by increased data rates transmission, since a lower proportion of signal components were included in CSI signal. Therefore, to improve the precision of CSI estimation under M-OOK signal with different data rates, a dynamic cut-off frequency of LPF is required.

Figure 6 demonstrates the BERs of various threshold decision methods under data rate of 10 Mbps. ATD based on LPF and FCNN cascading and FCNN-based adaptive LPF cut-off frequency were evaluated under conditions with σ_1^2 values of 0.0596, 0.2086, 0.2080, 0.4286, and 0.7248. Additionally, they were compared to theoretical ATD with ideal CSI knowledge, ATD accompanied with LPF of fixed cut-off frequency, and single ATD based on FCNN. For ATD accompanied with LPF of fixed cut-off frequency method, the frequency was configured to 1 kHz based on Figure 5. Due to the large proportion of signal components in the estimated CSI signal, its BER performance was limited. For the ATD technology based on a single FCNN, the obtained BER performance was poorer

Figure 8 BERs of proposed methods at $\sigma_{\rm I}^2$ of (a) 0.0596, (b) 0.2080, (c) 0.4286, (d) 0.7248 under 50 Mbps signal transmission



compared to other methods because it was difficult to obtain CSI knowledge with high accuracy using a single FCNN model. The proposed cascaded LPF and FCNN method involves grading with an FCNN model after the LPF, with a cut-off frequency of 1 kHz. This CSI extraction method reduced the signal complexity and LPF noises, and improved BER performance and the accuracy of extracted CSI knowledge. However, under different turbulent channels, the BER performance was inferior to theoretical ATD due to the limitation of the fixed cut-off frequency. Regarding the FCNN-based adaptive LPF cut-off frequency method, FCNN model was adopted to adaptively determine the optimized cut-off frequency. Figure 7 shows the optimized cut-off frequency selection in the spectrum of M-OOK signal in the circumstances of σ_1^2 at 0.0596. The FCNN model was applied after LPF to study the frequency features of M-OOK signal, and the frequency component with maximum value is selected as the optimal cut-off frequency in LPF. The results indicate that BERs of FCNN-based adaptive LPF cut-off frequency are close to that of theoretical ATD.

Figure 8 illustrates BERs of the proposed LPF and FCNN cascading and FCNN-based adaptive LPF cut-off frequency under 50 Mbps M-OOK signal transmission. They were analyzed under conditions with $\sigma_{\rm I}^2$ values of 0.0596, 0.2080, 0.4286, and 0.7248. Additionally, the comparison was conducted with theoretical ATD with ideal CSI knowledge, ATD based on LPF, and ATD based on FCNN. With regard to ATD based on LPF method, the cut-off frequency was configured to 20 kHz based on Figure 5. Similar BER performance was achieved at 50 Mbps M-OOK signal transmission compared to Figure 7. Therefore, BERs of FCNN-based adaptive LPF cut-off frequency are effective under varying data rates and turbulence channel intensities.

The degree of accuracy and computational complexity were analyzed for ATD based on FCNN, LPF, and FCNN cascading, and FCNN-based adaptive LPF cut-off frequency under different data rates and turbulence channel intensities. As shown in Tables 3–8, the FCNN-based adaptive cut-off frequency for LPF exhibits the highest accuracy, as the optimized LPF cut-off frequency effectively reduces the noise degree and signal processing complexity by FCNN model. Nonetheless, due to the additional cut-off frequency optimization process, this method

Table 3

Degree of accuracy and complexity under ATD based on FCNN at 10 Mbps signal transmission

Channel	Accuracy rate	Training time
$\sigma_I^2 = 0.0596$	85.51%	72 s
$\sigma_I^2 = 0.2080$	85.02%	70 s
$\sigma_I^2 = 0.4286$	87.12%	70 s
$\sigma_I^2 = 0.7248$	86.69%	72 s

Table 4
Degree of accuracy and complexity under LPF and FCNN cascading at 10 Mbps signal transmission

Channel	Accuracy rate	Training time
$\sigma_I^2 = 0.0596$	91.95%	69 s
$\sigma_I^2 = 0.2080$	91.82%	65 s
$\sigma_I^2 = 0.4286$	91.49%	65 s
$\sigma_I^2 = 0.7248$	90.69%	66 s

Table 5
Degree of accuracy and complexity under FCNN-based adaptive
HPL cut-off frequency at 10 Mbps signal transmission

Channel	Accuracy rate	Training time
$\sigma_I^2 = 0.0596$	96.69%	73 s
$\sigma_I^2 = 0.2080$	95.17%	71 s
$\sigma_I^2 = 0.4286$	95.98%	72 s
$\sigma_I^2 = 0.7248$	94.78%	69 s

Table 6
Degree of accuracy and complexity under ATD based on FCNN at 50 Mbps signal transmission

Channel	Accuracy rate	Training time
$\sigma_I^2 = 0.0596$	88.96%	980 s
$\sigma_I^2 = 0.2080$	87.93%	996 s
$\sigma_I^2 = 0.4286$	88.25%	989 s
$\sigma_I^2 = 0.7248$	89.47%	993 s

Table 7
Degree of accuracy and complexity under LPF and FCNN cascading at 50 Mbps signal transmission

Channel	Accuracy rate	Training time
$\sigma_I^2 = 0.0596$	95.68%	975 s
$\sigma_I^2 = 0.2080$	95.11%	962 s
$\sigma_I^2 = 0.4286$	94.28%	985 s
$\sigma_I^2 = 0.7248$	95.75%	976 s

Table 8
Degree of accuracy and complexity under FCNN-based adaptive
HPL cut-off frequency at 50 Mbps signal transmission

Channel	Accuracy rate	Training time
$\sigma_I^2 = 0.0596$	98.45%	1095 s
$\sigma_I^2 = 0.2080$	97.85%	1042 s
$\sigma_I^2 = 0.4286$	99.02%	1032 s
$\sigma_I^2 = 0.7248$	98.89%	1024 s

consumes relatively longer training time. Therefore, the proposed FCNN-based adaptive LPF cut-off frequency can efficiently compensate turbulence effect in the circumstance of various turbulent channel conditions and data rates. In future work, we will explore other DL model application, FCNN model optimization, and computational complexity reduction.

5. Conclusion

In summary, we have proposed an ATD technique for FSO communication, which was based on DL model and LPF. For the cascaded LPF and FCNN approach, the FCNN model was utilized to estimate the CSI of signals processed by fixed cut-off frequency-based LPF. Regarding FCNN-based adaptive HPL cut-off frequency technique, FCNN model was employed to adaptively determine the values of cut-off frequency. This technique was analyzed by comparing ATD with ideal CSI, ATD with fixed cut-off frequency configured HPF, and ATD based on FCNN in the situation of different degrees of data rates and scintillation effects. The proposed

methods were verified through simulation. The simulation results indicated that FCNN-based adaptive HPL cut-off frequency technique outperforms the ATD with fixed cut-off frequency configured HPF, ATD based on FCNN, and LPF and FCNN cascading method. Besides, it approaches the performance of ATD with ideal CSI across various degrees of data rates and turbulence channels. Therefore, this is a highly promising technique for FSO links.

Recommendations

This study proposes ATD technique assisted by DL model and LPF. Among various DL models, FCNN model is introduced. In the cascaded LPF and FCNN approach, FCNN model is deployed after LPF is configured with fixed cut-off frequency. Regarding FCNN-based adaptive LPF cut-off frequency technique, FCNN model is utilized to dynamically determine the cut-off frequency of LPF according to the variation of turbulence channel and data rate.

Funding Support

This work was supported by the 2023 Liaoning Provincial Department of Education General Program (JYTMS20231214).

Ethical Statement

This study does not contain any studies with human or animal subjects performed by any of the authors.

Conflicts of Interest

The authors declare that they have no conflicts of interest to this work.

Data Availability Statement

Data are available from the corresponding author upon reasonable request.

Author Contribution Statement

Yan Gao: Writing – original draft. Yan-Qing Hong: Conceptualization, Methodology, Software, Validation, Formal analysis, Investigation, Resources, Data curation, Visualization, Supervision, Project administration, Funding acquisition. Chao-Yue Zhai: Writing – original draft, Writing – review & editing. Xiao-Xue Ren: Writing – review & editing.

References

- [1] Elsayed, E. E. (2024). Atmospheric turbulence mitigation of MIMO-RF/FSO DWDM communication systems using advanced diversity multiplexing with hybrid N-SM/OMI M-ary spatial pulse-position modulation schemes. *Optics Communications*, 562, 130558. https://doi.org/10.1016/j.optcom.2024.130558
- [2] Yousif, B. B., Elsayed, E. E., & Alzalabani, M. M. (2019). Atmospheric turbulence mitigation using spatial mode multiplexing and modified pulse position modulation in hybrid RF/FSO orbital-angular-momentum multiplexed based on MIMO wireless communications system. *Optics Communications*, 436, 197–208. https://doi.org/10.1016/j.optcom.2018.12.034
- [3] Elsayed, E. E., & Yousif, B. B. (2020). Performance evaluation and enhancement of the modified OOK based IM/DD

- techniques for hybrid fiber/FSO communication over WDM-PON systems. *Optical and Quantum Electronics*, *52*(9), 385. https://doi.org/10.1007/s11082-020-02497-0
- [4] Hamza, A. S., Deogun, J. S., & Alexander, D. R. (2019). Classification framework for free space optical communication links and systems. *IEEE Communications Surveys & Tutorials*, 21(2), 1346–1382. https://doi.org/10.1109/COMST. 2018.2876805
- [5] Safi, H., Sharifi, A. A., Dabiri, M. T., Ansari, I. S., & Cheng, J. (2019). Adaptive channel coding and power control for practical FSO communication systems under channel estimation error. *IEEE Transactions on Vehicular Technology*, 68(8), 7566–7577. https://doi.org/10.1109/TVT.2019.2916843
- [6] Shin, W. H., Choi, J. Y., & Han, S. K. (2019). Fixed threshold on-off keying differential detection for satellite optical communications. *Optics Express*, 27(2), 1590–1596. https:// doi.org/10.1364/OE.27.001590
- [7] Wang, Z., Zhong, W. D., & Yu, C. (2011). Dynamic decision threshold and adaptive coherent detection in FSO communication system. In 2011 8th International Conference on Information, Communications & Signal Processing, 1–5. https://doi.org/10.1109/ICICS.2011.6174253
- [8] Nguyen, T. V., Le, H. D., & Pham, A. T. (2022). Echo state network for turbulence-induced fading channel prediction in free-space optical systems. In 2022 5th World Symposium on Communication Engineering, 47–52. https://doi.org/10.1109/ WSCE56210.2022.9916027
- [9] Ding, S., Zhang, J., & Dang, A. (2017). Adaptive threshold decision for on-off keying transmission systems in atmospheric turbulence. *Optics Express*, 25(20), 24425–24436. https://doi.org/10.1364/OE.25.024425
- [10] Jing, Q. W., Yu, P. Z., Lv, H. L., & Hong, Y. (2023). Turbulence-tolerant manchester on-off keying transmission for free-space optical communication. *Current Optics and Photonics*, 7(4), 345–353. https://doi.org/10.3807/COPP.2023.7.4.345
- [11] Riediger, M. L. B., Schober, R., & Lampe, L. (2009). Fast multiple-symbol detection for free-space optical communications. *IEEE Transactions on Communications*, 57(4), 1119–1128. https://doi.org/10.1109/TCOMM.2009. 04.070118
- [12] Aveta, F., Refai, H. H., & Lopresti, P. G. (2020). Cognitive multi-point free space optical communication: Real-time users discovery using unsupervised machine learning. *IEEE Access*, 8, 207575–207588. https://doi.org/10.1109/ACCESS. 2020.3038624
- [13] Wang, D., Zhang, M., Fu, M., Cai, Z., Li, Z., Han, H., ..., & Luo, B. (2016). Nonlinearity mitigation using a machine learning detector based on *k*-nearest neighbors. *IEEE Photonics Technology Letters*, 28(19), 2102–2105. https://doi.org/10.1109/lpt.2016.2555857
- [14] LeCun, Y., Bengio, Y., & Hinton, G. (2015). Deep learning. Nature, 521(7553), 436–444. https://doi.org/10.1038/nature14539
- [15] Palitharathna, K. W. S., Suraweera, H. A., Godaliyadda, R. I., Herath, V. R., & Thompson, J. S. (2022). Neural network-based channel estimation and detection in spatial modulation VLC systems. *IEEE Communications Letters*, 26(7), 1598–1602. https://doi.org/10.1109/LCOMM.2022.3166221
- [16] Amirabadi, M. A. (2019). A deep learning based solution for imperfect CSI problem in correlated FSO communication channel. arXiv Preprint: 1909.11002. https://doi.org/10. 48550/ARXIV.1909.11002
- [17] Du, Z., Deng, H., Dai, Y., Hua, Y., Jia, B., Qian, Z., ..., & Xu, J. (2022). Experimental demonstration of an OFDM-UWOC

- system using a direct decoding FC-DNN-based receiver. *Optics Communications*, 508, 127785. https://doi.org/10.1016/j.optcom.2021.127785
- [18] Li, J., Zhang, M., Wang, D., Wu, S., & Zhan, Y. (2018). Joint atmospheric turbulence detection and adaptive demodulation technique using the CNN for the OAM-FSO communication. *Optics Express*, 26(8), 10494–10508. https://doi.org/10.1364/ OE.26.010494
- [19] Doster, T., & Watnik, A. T. (2017). Machine learning approach to OAM beam demultiplexing via convolutional neural networks. *Applied Optics*, 56(12), 3386–3396. https://doi. org/10.1364/AO.56.003386
- [20] Tian, Q., Li, Z., Hu, K., Zhu, L., Pan, X., Zhang, Q., ..., & Xin, X. (2018). Turbo-coded 16-ary OAM shift keying FSO communication system combining the CNN-based adaptive demodulator. *Optics Express*, 26(21), 27849–27864. https://doi.org/10.1364/OE.26.027849
- [21] Darwesh, L., & Kopeika, N. S. (2020). Deep learning for improving performance of OOK modulation over FSO turbulent channels. *IEEE Access*, 8, 155275–155284. https:// doi.org/10.1109/ACCESS.2020.3019113
- [22] Hong, Y. Q., Li, G., & Liu, Z. Y. (2021). Optical adaptive power transmission using APC-EDFA for turbulence-tolerant FSO communications. *Optics Express*, *29*(15), 23777–23785. https://doi.org/10.1364/OE.431302
- [23] Al-Habash, A., Andrews, L. C., & Phillips, R. L. (2001). Mathematical model for the irradiance probability density function of a laser beam propagating through turbulent

- media. *Optical Engineering*, 40(8), 1554–1562. https://doi.org/10.1117/1.1386641
- [24] Dabiri, M. T., & Sadough, S. M. S. (2017). Generalized blind detection of OOK modulation for free-space optical communication. *IEEE Communications Letters*, 21(10), 2170–2173. https://doi.org/10.1109/LCOMM.2017.2722472
- [25] Dessen, F. (2019). Optimizing order to minimize low-pass filter lag. Circuits, Systems, and Signal Processing, 38(2), 481–497. https://doi.org/10.1007/s00034-018-0877-6
- [26] Qiu, J., Liu, W., Zhang, X., Li, E., Zhang, L., & Li, X. (2025). DED-SAM: Adapting segment anything model 2 for dual encoder–decoder change detection. *IEEE Journal of Selected Topics in Applied Earth Observations and Remote Sensing*, 18, 995–1006. https://doi.org/10.1109/JSTARS.2024.3490754
- [27] Pouyanfar, S., Sadiq, S., Yan, Y., Tian, H., Tao, Y., Reyes, M. P., ..., & Iyengar, S. S. (2019). A survey on deep learning: Algorithms, techniques, and applications. ACM Computing Surveys, 51(5), 92. https://doi.org/10.1145/3234150
- [28] Ibrahim, D. R. (2022). Design and optimization of butterworth and elliptic band pass filters in 5G application. *Al-Rafidain Engineering Journal*, *27*(2), 68–81. https://doi.org/10.33899/rengj.2022.132518.1146

How to Cite: Gao, Y., Hong, Y.-Q., Zhai, C.-Y., & Ren, X.-X. (2025). Deep Learning and LPF-Based Decision Technique in Free-Space Optical Communication Links. *Journal of Optics and Photonics Research*. https://doi.org/10.47852/bonviewJOPR52024917